NANO LETTERS

2008
Vol. 8, No. 2
478−484

Probing Molecules in Integrated Silicon–Molecule–Metal Junctions by Inelastic Tunneling Spectroscopy

Wenyong Wang,[†] Adina Scott,[‡] Nadine Gergel-Hackett,[†] Christina A. Hacker,[†] David B. Janes,*[,‡] and Curt A. Richter*[,†]

Semiconductor Electronics Division, National Institute of Standards and Technology, Gaithersburg, Maryland 20899, and School of Electrical and Computer Engineering and Birck Nanotechnology Center, Purdue University, West Lafayette, Indiana 47907

Received October 2, 2007; Revised Manuscript Received December 22, 2007

ABSTRACT

Molecular electronics has drawn significant attention for nanoelectronic and sensing applications. A hybrid technology where molecular devices are integrated with traditional semiconductor microelectronics is a particularly promising approach for these applications. Key challenges in this area include developing devices in which the molecular integrity is preserved, developing in situ characterization techniques to probe the molecules within the completed devices, and determining the physical processes that influence carrier transport. In this study, we present the first experimental report of inelastic electron tunneling spectroscopy of integrated metal–molecule–silicon devices with molecules assembled directly to silicon contacts. The results provide direct experimental confirmation that the chemical integrity of the monolayer is preserved and that the molecules play a direct role in electronic conduction through the devices. Spectra obtained under varying measurement conditions show differences related to the silicon electrode, which can provide valuable information about the physics influencing carrier transport in these molecule/Si hybrid devices.

Recently there has been great interest in incorporating molecular elements into electronic devices for electronics, high-density memory, and chemical/biological sensing applications. Such an approach is attractive because device properties can be tailored by modifying the chemical structures of the molecules directly, leading to flexible and scaleable fabrication schemes. To date much of the work that has been done on this topic has focused on self-assembled monolayers or individual molecules on metal electrodes.[1,2] However, replacing metal contacts with semiconductors presents significant physical and technological advantages.[3−8] Semiconductor surfaces can be functionalized by using a variety of covalent reactions, leading to stable and high quality monolayer formations.[3,9−10] Unlike metals, the electronic properties of semiconductors can be tailored through doping, considerably expanding the possibilities for device performance. Moreover, the interaction between the semiconductor bands and molecular energy levels can also lead to novel device behavior.[8] From a technological perspective, it is especially desirable to develop solid-state molecular devices based on silicon (Si) such as metal−molecule−silicon (MMS) devices, because the processing infrastructure and physical insights that have been developed for traditional integrated circuits can be utilized for such hybrid devices.

For solid-state molecular devices, one key challenge is to create a reliable top contact that is mechanically robust and integrated, yet does not destroy the molecular layer. In this study, this difficulty is addressed by depositing the top metallic contact by using a low-energy, indirect path evaporation technique.[11−12] In this "soft" deposition process, because of the system setup the metal must first scatter off the gas in the chamber before landing on the sample surface, thereby decreasing the kinetic energy of the impinging metal particles and minimizing the amount of damage and metal penetration in the organic layer. Another more demanding and critical issue toward realizing practical, reliable molecular electronic devices is to develop in-situ characterization techniques that can verify the presence and chemical integrity of the molecules in the completed device, as fabrication processes and metal−molecule interactions can lead to undesirable effects such as metal penetration and carbide formation.[13] Traditional techniques for analyzing monolayer quality such as X-ray photoelectron spectroscopy (XPS) and scanning probe techniques are surface specific. Spectroscopic measurements of buried molecular layers can be performed,[14] but they require device areas on the order of millimeters squared, which are unsuitable for integrated MMS devices

* Corresponding authors. E-mail: (D.B.J.) janes@ecn.purdue.edu; (C.A.R.) curt.richter@nist.gov.
[†] National Institute of Standards and Technology.
[‡] Purdue University.

10.1021/nl0725289 CCC: $40.75
Published on Web 01/12/2008

in the micro- or nanoscale. Inelastic electron tunneling spectroscopy (IETS) is an important nondestructive characterization technique that gives crucial information about the vibrational spectrum of the material in a junction.[15,16] This technique has recently been applied to metal−molecule−metal (MMM) junctions and has shown direct evidence of a dominant conduction path though molecular states, as well assisted in developing a clear physical picture of intrinsic molecular transport in such structures.[17−20] In this study, we utilize this technique for the first time to investigate solid-state MMS devices with the molecules assembled directly on silicon surfaces. For such structures, IETS is especially crucial because, unlike in MMM devices where failures due to metal penetration through the monolayer will show up as short circuits that are evident in current−voltage ($I-V$) measurements, in MMS devices such failures can form metal-semiconductor contacts and still yield appealing electrical characteristics, making it extremely difficult to distinguish true molecular effects from $I-V$ characterizations alone. In our study, we have utilized IETS characterization to verify that the molecular integrity is preserved in the fabricated hybrid silicon-based molecular structures and to demonstrate chemically specific effects of the molecular layers on transport, which can provide important insight into the mechanisms of interaction between the charge carriers and the molecule of interest in this class of devices. Several aspects of the spectra are different than typically found on MMM devices, including the observation of peaks associated with the Si electrode as well as bias asymmetry and broadening of the intrinsic line width of the peaks.

In IETS, the vibrational modes of the molecular species present are detected by their influence on the current through a tunnel barrier. The signature of a molecular vibration coupled to an electronic level is a change of slope in the $I-V$ characteristic of the device, which appears as a peak in the second derivative. The IETS spectra can be measured directly by exciting the device with a small alternating current (ac) modulation while sweeping the direct current (dc) bias and measuring the second harmonic of the ac signal.[17] For MMS devices, the mechanisms for conduction can vary depending on electrostatic considerations,[7] therefore special considerations must be taken to design a device that is suitable for IETS measurements. First, there must be sufficient carrier density in the Si contact at low temperatures, which requires a high doping density. Second, it is desirable to have minimal offset between the Si Fermi energy and the metal work function, because the presence of a semiconductor depletion region will result in a situation where the molecular layer mainly acts as a perturbation on a Schottky barrier. To address these concerns, the devices in this study were all fabricated using p+ ($N_a = 4 \times 10^{19}$ cm^{-3}) Si substrates with gold top contacts. The doping condition of the metal−insulator transition for Si at $T = 4$ K is 4×10^{18} cm^{-3}, therefore the above doping density is sufficient that the Si substrate can be treated in a manner theoretically similar to a metal, although additional physical effects may arise from the relatively low density of states in the Si and the fact that the number of charge carriers is modest. We choose gold as the metal contact because its work function and the Si valence band are at similar energies, which gives a near flat-band electrostatic condition where the semiconductor depletion effects will be minimal and the molecules will be the primary current-limiting mechanism.[7]

Silicon−molecule−gold devices were fabricated using traditional silicon-processing techniques with appropriate modifications to enable the incorporation of molecular monolayers.[7] p+ ($N_a = 4 \times 10^{19}$ cm^{-3}) ⟨111⟩ silicon substrates were coated with a 50 nm thermal oxide and 200 nm of silicon nitride. Standard photolithography was used to define well patterns that have dimensions ranging from (2×2) μm^2 to (11×11) μm^2. The nitride was etched by using reactive ion etching and the oxide was etched by using buffered oxide etch. The photoresist was then stripped and the samples were cleaned in solvents followed by piranha solution. Prior to surface modification, the samples were etched in deoxygenated ammonium fluoride for 12 min to hydrogen terminate the silicon surface in the wells. Octadecane monolayers were grafted to Si by thermal reaction of octadecene solution with the hydrogen-terminated Si surface.[21] Substituted aromatic molecular monolayers were grafted by electrochemical reduction of diazonium salts in acidic aqueous solutions.[10] After the surface modification was completed, the samples were cleaned with dichloromethane or acetonitrile using ultrasonication to remove physisorbed molecular species and reaction byproducts. Molecular layers were grafted to unpatterned Si samples and characterized by using XPS, Fourier transform infrared (FTIR), ellipsometry, contact angle measurements, and atomic force microscopy to verify the presence of the molecular species of interest. It was determined that octadecene and D-benz form relatively ideal, well-ordered monolayers. N-benz forms somewhat more disordered monolayers with a submonolayer amount of oxide. Top contact metallization was performed by using the soft gold evaporation technique.[11−12] The samples were placed in the chamber of a thermal evaporator facing away from the source. The chamber is pumped down to 10^{-6} Torr and then backfilled with argon to atmospheric pressure. This pump−purge cycle was repeated to remove impurities from the chamber that may affect film quality. Then, the chamber was pumped to 6 mTorr, and the evaporation was performed. A crystal monitor placed next to the samples facing away from the source material was used to monitor the deposition. Approximately 20 nm of gold was deposited by using this method. Standard electron-beam evaporation was then used to deposit a thick (200 nm) layer of gold to enable further processing. Contact pads were defined by using standard photolithography and a commercial gold etchant. A gold ohmic back contact was applied by using electron-beam evaporation. A schematic of the device is shown in Figure 1. Two types of molecular layers have been chosen for this study: one is octadecane (C18), one of the alkyl molecules that has been studied extensively and has been used as a model molecular species in metal-based molecular electronics testbeds;[22] the other type includes nitrobenzene (N-benz) and diethylaminobenzene (D-benz), which are aromatic mol-

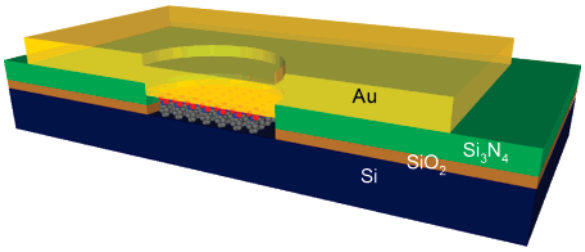

Figure 1. Schematic of the integrated silicon−organic molecule−metal device. The thicknesses of the SiO_2 and silicon nitride insulating layers are 50 and 200 nm, respectively. The well patterns have dimensions ranging from (2 × 2) to (11 × 11) μm^2.

ecules that have been calculated to show different energy band lineups with the contact Fermi energies and that exhibit significantly different transport behavior in MMS devices.[7] The chemical structures of the molecular species are shown with their respective IETS spectra in Figure 2.

Inelastic electron tunneling spectra of the samples were obtained via direct lock-in second harmonic measurements.[17] Figure 2a shows the representative IETS spectrum of an integrated Si-C18-Au device measured at 4.2 K. An ac modulation of 7.8 mV (root-mean-square value) at a frequency of 1033 Hz was applied to the device to acquire the second harmonic signal. Measurements at different dc resolutions and ac modulations were also performed to confirm the validity of the observed IETS spectra. IETS for devices with N-benz and D-benz molecular layers are shown in Figure 2, panels b and c, respectively. The spectra were interpreted by comparing the peak energies with previously reported vibrational energies from molecular dynamics simulations and infrared, Raman, and IETS measurements. The observed peaks are attributed to vibrational modes associated with the molecular layer or the silicon contact and the mode assignments are given in Table 1.

There are some features that are common to all of the spectra: a silicon phonon mode is observed at ∼60 mV and a Si−H stretch is seen at ∼260 mV in all samples. The Si peak comes from lattice vibrations of the crystalline silicon electrode. The ideal packing density of the molecular layers is on every other silicon site on the ⟨111⟩ surface, and the presence of the Si−H stretch signal suggests that the interstitial sites remain largely hydrogen-terminated. A similar pronounced IETS peak due to Si−H vibration has also been observed from characterization of thin amorphous Si−H films.[26] XPS studies of the aryl molecular layers on unpatterned substrates reveal submonolayer amounts of silicon oxide present on the surface in addition to the molecular modifier of interest.[7] FTIR studies of the C18 layers show small amounts of silicon oxide present in these layers as well. In IETS, however, SiO_x modes that would be expected at energies in the range of 130−160 mV[16,23] are not observed. The absence of these peaks indicates the molecular layers are in fact grafted directly to the silicon surface and that the small amount of oxide present in the devices does not play a significant role in transport.

The observation of peaks in the various IETS spectra corresponding to vibronic modes of the respective molecular

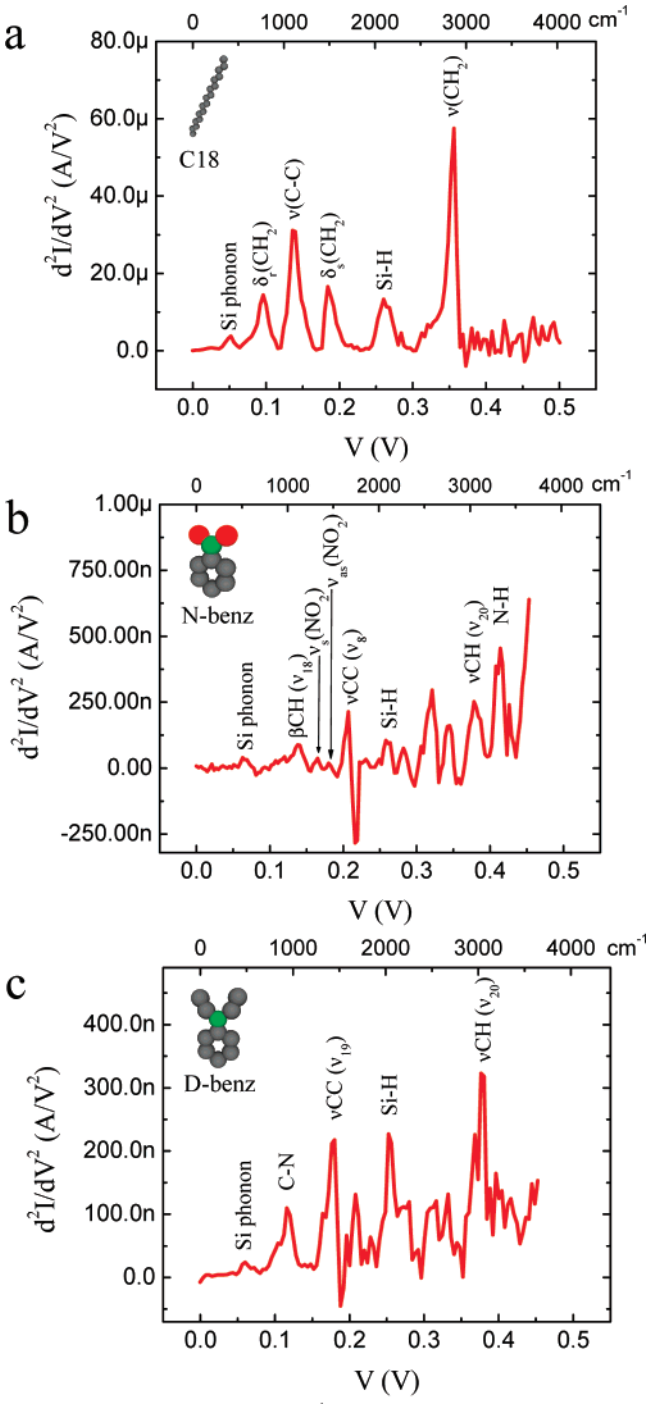

Figure 2. Representative IETS spectra of the hybrid Si-based devices containing (a) octadecane (C18), (b) nitrobenzene (N-benz), and (c) diethylaminobenzene (D-benz) molecules obtained at 4.2 K. The dominant peaks are identified as contributions from the molecular vibrational modes indicated in the plots. The insets show the chemical structures of the respective molecules.

species provides clear evidence of the existence of the desired molecular species in the fabricated hybrid junctions. For the aromatic samples, the spectra display characteristic vibrational peaks of the different derivatives of the aromatic ring, that is, the peaks at 165 and 180 mV associated with the NO_2 substituant in the N-benz device and the C−N peak at 116 mV associated with the $N(CH_3)_2$ substituant in the D-benz device, confirming the existence of the specific

Table 1. Vibrational Mode Assignments for IETS Spectra of MMS Devices[a]

molecular species	peak position (mV)	mode assignment	refs
C18	*52*	*Si phonon*	16,23
	96	**CH_2 in-plane rocking**	17,24
	136	**C-C stretching**	17,24
	184	**CH_2 in-plane scissoring**	17,24
	260	*Si-H*	25,26
	356	**CH_2 stretching**	17,24
N-benz	*63*	*Si phonon*	16,23
	138	**C-H (ν_{18}) ring mode**	24,27,28
	165	**NO_2 symmetric stretch**	29
	180	**NO_2 asymmetric stretch**	29
	207	**C-C (ν_8) ring mode**	24,27,28
	258	*Si-H*	25,26
	282	undetermined	
	345	undetermined	
	378	**C-H (ν_{20}) ring mode**	24,27,28
	414	**N-H stretch**	10,24
D-benz	*60*	*Si phonon*	16,23
	116	**C-N**	10,24
	180	**C-C (ν_{19}) ring mode**	24,27,28
	252	*Si-H*	25,26
	376	**C-H (ν_{20}) ring mode**	24,27,28

[a] Modes shown in bold are molecular vibrations. Modes shown in italics are associated with the silicon contact.

molecules in the integrated junctions. XPS studies of nitro-containing layers on Si indicate that the NO_2 headgroup can be reduced to form NO_x and NH_x species (see Supporting Information). For the N-benz device, the peak at 414 mV (Figure 2b) is attributed to the presence of NH-substituted benzene in the molecular layer; the peaks at 282 and 385 mV were not assigned to any known modes based on the literature. The spectra for both substituted benzene molecules exhibit features with a peak−valley shape near 200 mV assigned to the C−C ring modes, which might indicate that molecular level-assisted transport is occurring through the delocalized π-electron systems of these molecules.[19]

Because of the electronic structure of the silicon electrode, one would speculate that the IETS spectra of Si-based molecular devices would be in some way different from those of MMM systems. In addition to the observation of Si modes, potential differences might include selection rules for peaks, bias-related effects, and electric field effects. Additional measurements were performed on the Si-C18-Au devices to explore possible effects related to the Si electrode. Figure 3a shows the spectra for the Si−C18−Au devices measured at different temperatures (4.2, 20, and 35 K), exhibiting the thermal broadening effect of the spectral lines at a fixed ac modulation (7.8 mV). Spectra were also obtained at 4.2 K for different ac modulation amplitudes (see Supporting Information). In IETS, the line width of a vibrational peak can be broadened by the amplitude of the ac excitation signal and the thermal distribution of the carriers. A Gaussian fit to the spectra gives the full width at half-maximum of an individual peak. Following the procedure developed for MMM devices,[17] the intrinsic line width of the peak can then be calculated by compensating for the modulation broadening

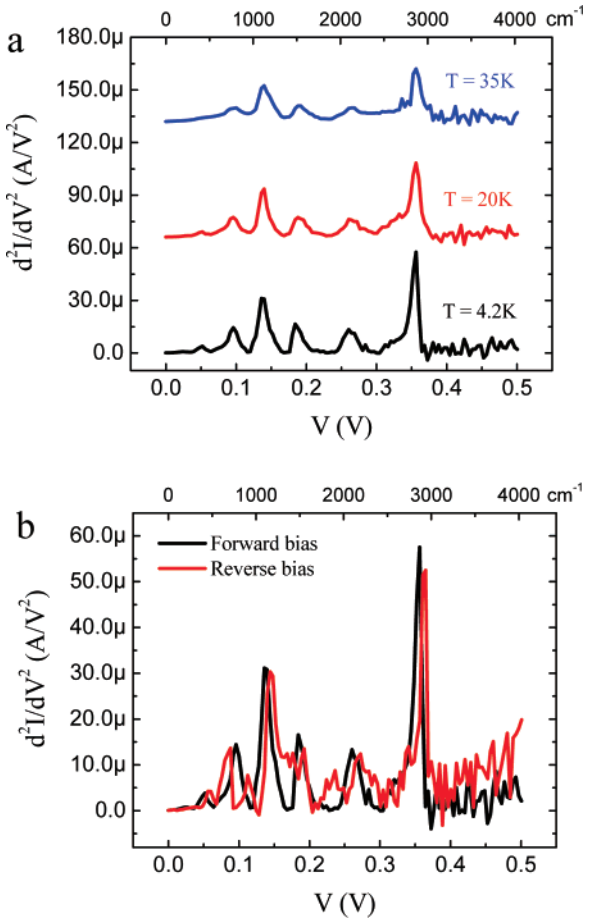

Figure 3. IETS spectra of the Si−C18−Au device obtained (a) at different temperatures (4.2, 20, and 35 K), showing the thermal broadening effect of the spectra lines, and (b) at different bias polarities.

(≈1.7 V_{ac}) and thermal broadening (≈ 5.4 k_BT) effects. The peak corresponding to the C−C stretching mode of the C18 device can be directly compared to prior results for this mode in a MMM junction.[17] After using the approach described elsewhere[17] to correct for modulation and thermal broadening, the intrinsic line width is calculated to be ~10 mV, about 3 times larger than that of a much shorter alkyl molecule (octanethiol) incorporated in an Au−Au junction.[17] The other molecular peaks in this spectrum show comparable measured linewidths, although the CH_2 peak exhibits a slightly smaller line width under the same measurement conditions. It should be noted that other studies of alkanethiols in MMM junctions have exhibited broader linewidths than those observed here for comparable measurement conditions, however detailed experimental data on the thermal and modulation broadening effects of these studies are not available.[18] Because of the lower signal levels present in the spectra of the aromatic molecules, it was difficult to accurately determine the linewidths and perform a comparison study. However, peak fits were conducted for the spectra obtained at 4.2 K and at a fixed modulation voltage of 7.8 mV, and the obtained intrinsic widths were in the range of 10−25 mV, comparable to those measured for C18.

Figure 3b shows the IETS spectra of the same C18 sample from Figure 3a obtained under forward and reverse biases

Table 2. Peak Shift of the C18 Device under Different Bias Polarities

mode	forward bias peak position (mV)	reverse bias peak position (mV)	Peak shift (mV)
Si phonon	52	56	4
$\delta_r(CH_2)$	96	112	16
ν(C-C)	136	144	8
$\delta_s(CH_2)$	184	192	8
Si-H	260	272	12
$\nu(CH_2)$	356	364	8

at 4.2 K. Compared to the forward-bias spectrum, the peak positions of the reverse-bias spectrum are shifted, and the shifts of the major identified peaks are given in Table 2. Almost all of the molecular modes observed in both spectra shifted by ~8 mV whereas the Si phonon mode and the Si−H mode shifted by 4 and 12 mV, respectively, which excludes the possibility that such shifts were caused by the asymmetry of the conductance or a voltage offset in the measurement setup. In metal oxide tunnel devices, IETS peak shifts on the order of 1 mV (2%) under different bias polarities have been reported.[30] The shifts have been attributed to the bias polarity-dependent changes in the molecular vibrational energy, that is, the large electrical fields of different polarities present in the tunnel junction perturb the vibrational frequency differently via anharmonic effects.[30] This effect alone, however, is not sufficient to explain the magnitude of the bias-dependent peak shifts observed in this study.

To gain more insight about MMS devices from the IETS characterizations, it is important to consider the process by which carriers are tunneling. Figure 4 is a band diagram of the Si−molecule−Au device, illustrating the expected conduction mechanisms under different bias directions. Note that the horizontal axes have been drawn approximately to scale for the C18 molecule, while for clarity the amount of band bending has been exaggerated with respect to the applied bias. The electronic properties of the p+ Si electrode were approximated by using a parabolic band effective density of state (DOS) with appropriate modifications to the usual Si band gap and DOS to take into account low temperature and high doping density effects.[31,32] At this doping density, the acceptor levels are expected to form an impurity band near the valence band edge, resulting in an effective shift in the valence band edge energy (E_V). Carrier freezeout is not observed at low temperatures in Si layers with comparable acceptor densities. The bulk Fermi energy (E_F) is estimated to be ~3.3 mV below E_V and the built-in potential is on the order of 20 mV (neglecting molecular and interface dipoles). Nonresonant tunneling is the primary conduction process in this measurement, so the detailed molecular density of states is not necessary for interpretation of the results.

The band diagrams in Figure 4 can be used to qualitatively explain factors that likely contribute to the peak shifts and broadening of the intrinsic linewidths observed in the MMS devices. Under forward bias, electrons below the metal Fermi energy can tunnel through the molecular layer into empty electron states (filled hole states) at energies between E_F and E_V in the Si. In this case, the onset of an IETS signal would

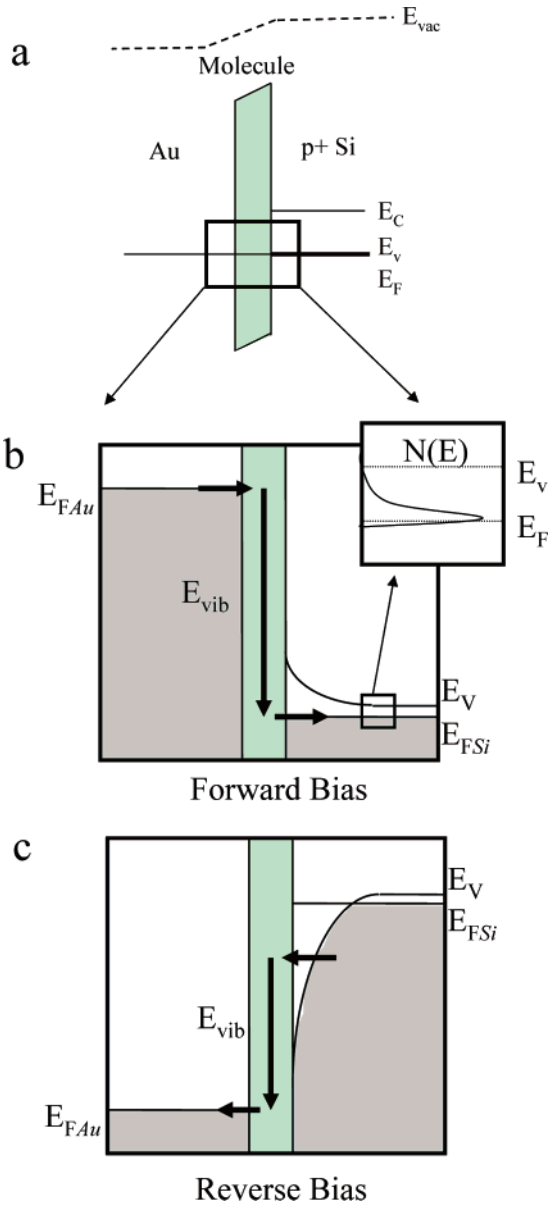

Figure 4. (a) Energy band diagram of the Si−molecule−Au device and schematics of possible conduction paths for (b) forward and (c) reverse biases. The inset in panel b illustrates the distribution of empty electron states N(E) in the valence band available for transport. The horizontal axes are drawn approximately to scale for the case of C18, but amount of band bending is exaggerated for clarity. E_{vib} illustrates the phonon energy that would be detected by IETS for a given applied bias, near the onset of the peak.

occur when the applied bias is approximately equal to the vibronic mode energy divided by electronic charge similar to the case for MMM devices, corresponding to the bias point illustrated in Figure 4b. Under reverse bias, electrons from filled (electron) states in the Si valence band can tunnel through the molecular layer into empty states in the metal (i.e., states above the metal E_F). Approximate electrostatic calculations indicate that band-bending of up to 80 meV with a spatial extent of up to 1.5 nm is occurring at the Si surface over the reported voltage range in reverse bias. This implies that electrons may be tunneling though this Si barrier with

a process similar to Fowler−Nordheim tunneling such that the effective injection energy is below the semiconductor Fermi energy, as illustrated schematically in Figure 4c. The inset to Figure 4b illustrates an approximate empty electron state distribution in which the rise between E_v and E_F is associated with the DOS and the fall near E_f is associated with the Fermi function. In this case, the onset of an IETS signal would occur at an applied voltage larger than the vibronic mode energy divided by electronic charge, corresponding to a shift of the reverse bias peaks toward larger voltage magnitudes, with respect to the forward bias peaks. In the forward-bias direction, however, there is no possibility of creating a depletion region, therefore inelastic processes analogous to the case of a MMM system can occur. In addition, due to the electronic properties of silicon including the band bending near the surface the electric field profile in MMS devices is different from other systems studied by IETS. The dielectric nature of the Si contact means that it does not screen fields like metal contacts do. This implies that strong local fields may be present, leading to field-effect shifts in a manner similar to metal-oxide devices. In addition, the local electric field profiles are different in the two bias directions.

Theoretical investigations have shown that intrinsic IETS linewidths in MMM devices are dominated by the couplings of molecular vibrations to the electronic and vibronic excitations in the electrodes.[19] In the MMS structures, the presence of a Si−C bond as opposed to an Au-thiol bond is likely to lead to stronger electronic and vibronic couplings between the molecule and the silicon electrode. The higher frequency of the silicon phonons would also lead to a stronger coupling between the molecular vibrations and the electrode's vibronic excitations.[33] The allowable range of injection energies under forward bias (Figure 4b) may also contribute to the observed broadening in the intrinsic line width of the IETS peaks. For the forward bias case considered in Figure 3a, changes in conductance should occur over a bias range required to sweep the metal Fermi level through the distribution of empty electron states in the silicon valence band, which occurs over an energy range of several meV as illustrated in the inset of Figure 4b. Therefore, IETS peaks in MMS devices should be broadened by an additional factor with respect to corresponding peaks in MMM devices in which the primary electronic broadening contributed by the contacts is expected to correspond to thermal broadening. These factors could jointly produce larger linewidths of the vibrational peaks, as manifested experimentally in the C−C stretching mode of the Si-C18-Au junction. Further theoretical and experimental investigations are in progress to fully understand these issues, which could provide critical information on the MMS tunnel junction environment.

In summary, IETS has been used to probe transport properties of molecular layers in integrated MMS devices with monolayers grafted directly to silicon for the first time. In the devices presented, appropriate doping has been used to achieve a situation where the molecular layer is the primary barrier to transport; therefore the present study offers important insight into intrinsic molecular conduction in such systems. Through the probing of several different molecular layers, chemical sensitivity was demonstrated by exploring the differences in the IETS spectra. Electronic features of the silicon contact and information about the molecular configuration were evident from the similarities in the spectra, which demonstrate the importance of this in situ technique for exploring molecular systems associated with semiconductors. Qualitative differences between the observed IETS spectra in MMS devices and those in MMM devices have been discussed. Spectra obtained under different bias polarities suggested that the presence of a semiconducting electrode influenced the electrostatics of the junction and could yield valuable information on the microscopic environmental situations in MMS tunnel junctions.

Acknowledgment. The authors would like to thank Kirk Bevan, Supriyo Datta, Siyuranga Koswatta, Mark A. Ratner, Chad Risko, Gemma Solomon, and Duncan R. Stewart for helpful discussions. Work at Purdue is supported by NSF (ECE0506802) and NASA-URETI (NCC3-1363). A.S. is supported by a NSF graduate research fellowship. Work at NIST is supported by the DARPA MoleApps Program and the NIST Office of Microelectronics Programs.

Supporting Information Available: XPS and FTIR spectra and a study of modulation broadening of IETS spectral linewidths. This material is available free of charge via the Internet at http://pubs.acs.org.

References

(1) Molecular Electronics: Science and Technology. In *The Annals of the New York Academy of Sciences*; Aviram, A., Ratner, M. A., Eds.; New York Academy of Sciences: New York, 1998; Vol. 852.
(2) Ulman, A. *An Introduction to Ultrathin Organic Films from Langmuir-Blodgett to Self-Assembly*; Academic Press: Boston, MA, 1991.
(3) Buriak, J. M. *Chem. Rev.* **2002**, *102*, 1271.
(4) Wang, W.; Lee, T.; Kamdar, M.; Reed, M. A.; Steward, M. P.; Huang, J. J.; Tour, J. M. *Superlattices Microstruct.* **2003**, *33*, 217−226.
(5) Miramond, C.; Vuillaume, D. *J. Appl. Phys.* **2004**, *96*, 1529−1536.
(6) Salomon, A.; Boecking, T.; Gooding, J. J.; Cahen, D. *Nano Lett.* **2006**, *6*, 2873−2876.
(7) Scott, A.; Risko, C.; Ratner, M. A.; Janes, D. B. *Appl. Phys. Lett.* **2007**, *91*, 033508.
(8) Guisinger, N. P.; Greene, M. E.; Basu, R.; Baluch, A. S.; Hersam, M. C. *Nano Lett.* **2004**, *4*, 55−59.
(9) Linford, M.; Fenter, P.; Eisenberger, P. M.; Chidsey, C. E. D. *J. Am. Chem. Soc.* **1995**, *117*, 3145−3155.
(10) Allongue, P.; de Villeneuve, C. H.; Pinson, J.; Ozanam, F.; Chazalviel, J. N.; Wallart, X. *Electrochim. Acta* **1998**, *43*, 2791−2978.
(11) Lodha, S.; Janes, D. B. *J. Appl. Phys.* **2006**, *100*, 024503.
(12) Metzger, R. M.; Xu, T.; Peterson, I. R. *J. Phys. Chem. B* **2001**, *105*, 7280−7290.
(13) Walker, A. V.; Tighe, T. B.; Stapleton, J.; Haynie, B. C.; Upilli, S.; Allara, D. L.; Winograd, N. *Appl. Phys. Lett.* **2004**, *84*, 4008.
(14) Richter, C. A.; Hacker, C. A.; Richter, L. J. *J. Phys. Chem. B* **2005**, *109*, 21836.
(15) Jaklevic, R. C.; Lambe, J. *Phys. Rev. Lett.* **1966**, *17*, 1139−1140.
(16) Petit, C.; Salace, G.; Lenfant, S.; Vuillaume, D. *Microelectron. Eng.* **2005**, *80*, 398−401.
(17) Wang, W.; Lee, T.; Kretzschmar, I.; Reed, M. A. *Nano Lett.* **2004**, *4*, 643−646.
(18) Kushmerick, J. G.; Lazorcik, J.; Patterson, C. H.; Shashidhar, R.; Seferos, D. S.; Bazan, G. C. *Nano Lett.* **2004**, *4*, 639−642.
(19) Galperin, M.; Ratner, M. A.; Nitzan, A. *Nano Lett.* **2004**, *4*, 1605−1611.

(20) Troisi, A.; Beebe, J. M.; Picraux, L. B.; van Zee, R. D.; Stewart, D. R.; Ratner, M. A.; Kushmerick, G. J. *Proc. Natl. Acad. Sci. U.S.A.* **2007**, *104*, 14255.
(21) Richter, C. A.; Hacker, C. A.; Richter, L. J.; Vogel, E. M. *Solid State Electron.* **2004**, *48*, 1747−1752.
(22) Wang, W.; Lee, T.; Reed, M. A. *Phys. Rev. B* **2003**, *68*, 035416.
(23) Lye, W.; Hasegawa, E.; Ma, T. P.; Barker, R. C.; Hu, Y.; Kuehne, J.; Frystak, D. *Appl. Phys. Lett.* **1997**, *71*, 2523−2525.
(24) Walmsley, D. G.; Tomlin, J. L. *Prog. Surf. Sci.* **1985**, *18*, 247−447.
(25) Oheda, H. *Phys. Rev. B* **1999**, *60*, 16531−16542.
(26) Higo, M.; Kamata, S. *Anal. Sci.* **2002**, *18*, 227−242.
(27) Avram, M.; Mateescu, G. D. *Infrared Spectroscopy: Applications in Organic Chemistry*; Wiley: New York, 1972.
(28) Varsanyi, G. *Assignments for vibrational spectra of 700 benzene derivatives*; John Wiley & Sons: New York, 1974.
(29) Korman, C. S.; Coleman, R. V. *Phys. Rev. B* **1977**, *15*, 1877−1893.
(30) Line, M. J.; Pritchard, R. G.; Oxley, D. P. *J. Phys.: Condens. Matter* **1989**, *1*, 6835−6842.
(31) Green, M. A.; *J. Appl. Phys.* **1990**, *67*, 2944−2954.
(32) Glass, G.; Kim, H.; Desjardins, P.; Taylor, N.; Spila, T.; Lu, Q.; Greene, J. E. *Phys. Rev. B* **2000**, *61*, 7628−7644.
(33) Galperin, M. Personal communications.

NL0725289